

A Platform-Tolerant Loop Antenna for Use On/Off Metal Ground Planes

John J. Borchardt, *Member, IEEE*

Abstract—Detuning of antennas due to changes in the surrounding environment can cause significant degradation in radio link range due to increased mismatch loss at the antenna feed. This paper shows that when an electrically small loop antenna is placed near a large conducting ground plane, mismatch loss is primarily caused by a shift in resonant frequency. Next, a loop antenna geometry that passively maintains its free-space tune and impedance when located a certain distance away from a large conducting ground plane is presented. An equivalent circuit model that explains this behavior is introduced. The circuit model shows that the geometry balances inductive and capacitive parasitics introduced by the ground plane such that the loop reactance and thus resonant frequency do not change. A design law based on the equivalent circuit is then derived. Finally, data showing a prototype loop antenna prevents frequency shift in practice is given.

Index Terms—Antennas, Radiofrequency identification (RFID), Loop antenna, Platform-tolerance, Metal tag

I. INTRODUCTION

Detuning of electrically small antennas due to changes in the environment surrounding the antenna can cause significant reduction in radio link range due to increased mismatch loss at the antenna feed, as is commonly observed in passive ultra-high frequency (UHF) radiofrequency identification (RFID) antennas [1], [2]. Many RFID antenna designs have been reported that are suitable for emplacement on metal; most often these geometries incorporate a low-permittivity foam spacer [3], a shielding cavity [4], an electromagnetic band-gap structure [5] or incorporate their own inherent ground plane [6]. Fewer geometries may be used equally in both free-space and near a ground plane such as the dipoles reported in [7] and [8]. In [9], researchers reported a folded, meandered half-wave dipole geometry with reduced impedance variation between free-space and ground plane environments. However, as the electrical size of the antenna is further reduced, even small perturbations in antenna impedance due to changes in the antenna environment can result in severe mismatch loss at the antenna feed. This paper presents a novel loop antenna

geometry whose free-space reactance is unchanged when placed a certain distance from a large conducting ground plane. As such, its tune and match are substantially constant in these two environments. This approach incurs none of the cost, size, complexity, RF loss or DC power consumption of active antenna tuning technologies.

II. DETUNING NEAR A GROUND PLANE

The severity and nature of the detuning problem for small loop antennas used in both free-space and near ground planes may be demonstrated via full-wave simulation of the copper loop antenna geometry shown in Fig. 1. At 433 MHz, this loop has electrical size $ka \sim 0.2$ (where k is the wavenumber and a is the radius of the smallest sphere enclosing the antenna). Accordingly, it has a high radiation Q and narrow impedance bandwidth and the realized antenna gain for fixed frequency radio services will critically depend on the ability of the antenna to maintain its tune and match despite environmental changes.

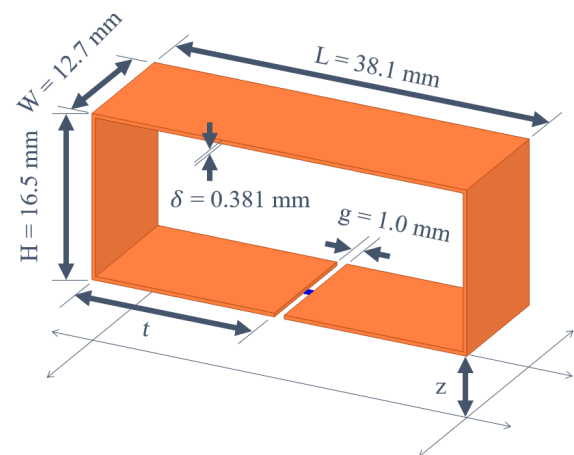


Figure 1. Copper loop antenna above an infinite ground plane. A wide conductor reduces both Ohmic losses and Q. The loop is fed at the $g=1.0$ mm gap and resonated and matched at 433 MHz for a free-space ($z=\infty$) environment. When it is placed near a ground plane, $z=1.27$ mm. Initially, the feed gap is centered on the bottom face of the loop ($t=18.55$ mm); in Section III, t will be changed to 7.2mm to eliminate detuning when $z=1.27$ mm.

This paragraph of the first footnote will contain the date on which you submitted your paper for review. [Current date 29-May-2019.]

John J. Borchardt is with Sandia National Laboratories, Albuquerque, NM 87185 USA (e-mail: jjborch@sandia.gov).

Sandia National Laboratories is a multimission laboratory managed and operated by National Technology and Engineering Solutions of Sandia, LLC, a

wholly owned subsidiary of Honeywell International, Inc., for the U.S. Department of Energy's National Nuclear Security Administration under contract DE-NA0003525. This paper describes objective technical results and analysis. Any subjective views or opinions that might be expressed in the paper do not necessarily represent the views of the U.S. Department of Energy or the United States Government.

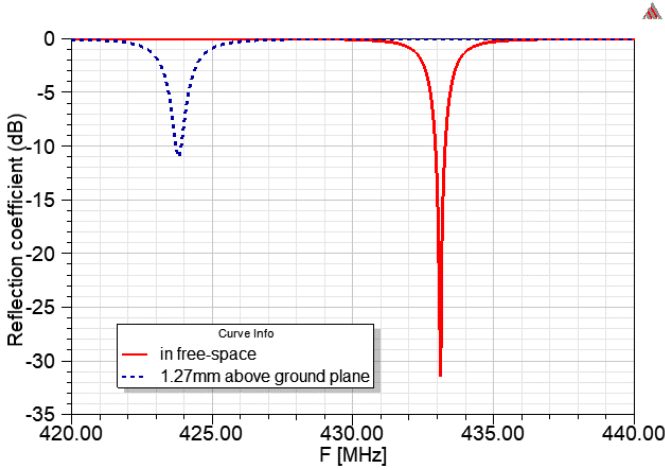


Figure 2. Reflection coefficient of the Fig. 1 loop with $t=18.55$ mm when matched for a free-space environment and when the same loop and same matching network is located $z=1.27$ mm above a ground plane. The ground plane shifts the resonance only 2% to 424MHz, but causes 20dB mismatch loss at 433 MHz.

The loop of Fig. 1 with $t=18.55$ mm is simulated both in free-space and $z=1.27$ mm away from a large ground plane using Ansys HFSS. The free-space loop is resonated and matched at 433 MHz with a network consisting of 4.19 pF and 149 pF ideal capacitors in series (the impedance across the larger capacitor is close to 50Ω at 433 MHz), resulting in the reflection characteristic shown in Fig. 2. When this *same loop and same matching network* is located $z=1.27$ mm away from a large ground plane, its impedance is perturbed and the resonance shifts 2% to 424MHz. In this state, the mismatch loss is greater than 20 dB at 433 MHz. However, near 424 MHz the antenna has only 0.5 dB mismatch loss—the issue is just a shift in the frequency at which the antenna is well-matched.

III. A LOOP ANTENNA WITH NO DETUNING

The loop of Fig. 1 is now altered such that $t=7.2$ mm. The full-wave calculated loop reactance without any matching network, X_{loop} , is plotted in Fig. 3(a) for the loop in free-space and $z=1.27$ mm away from the ground plane. Here, $X_{loop} = 90.7 \Omega$ at 433 MHz for both environments. As such, when the loop is resonated and matched at 433MHz with 4.17 pF and 148 pF ideal capacitors in series, the resonant frequency shifts negligibly between the two environments, as shown in Fig. 3(b). There is a modest change in the loop resistance R_{loop} between the environments (about 0.122Ω in free-space and 0.230Ω when $z=1.27$ mm away from the ground plane). However, the resulting mismatch loss is small in practice, as seen in Fig. 3(b).

The full-wave radiation efficiency of the loop alone is 57% in free-space and 76% when $z=1.27$ mm away from the ground plane; losses in the capacitive matching network may be considered separately. Because the loop circumference is only 16% of the wavelength, the current distribution is uniform. Consequently, the radiation pattern is a torroid in free-space and a half-torroid when very close to a large ground plane.

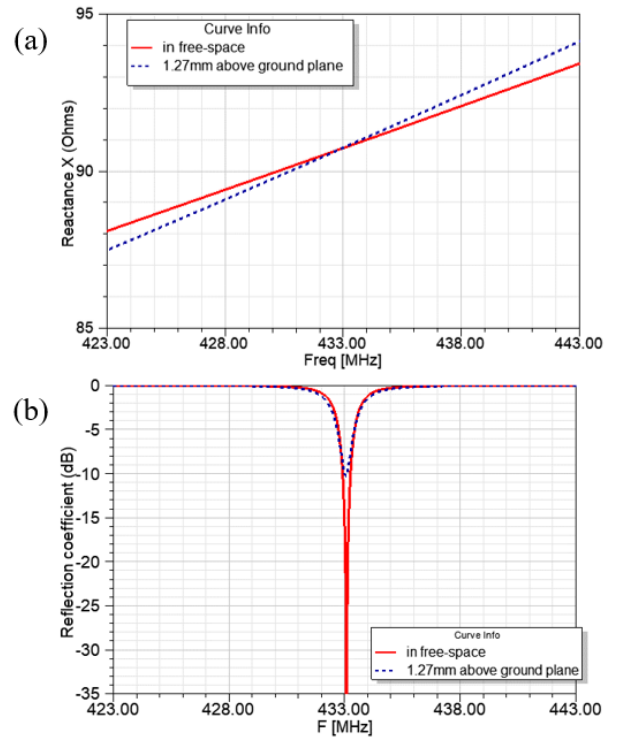


Figure 3. (a) full-wave, $t=7.2$ mm loop reactance (with no matching network) in free space and $z=1.27$ mm above a ground plane. The reactance in both environments is equal at 433 MHz. (b) matched, $t=7.2$ mm loop reflection characteristic for free-space and $z=1.27$ mm above a ground plane, showing negligible detuning between the two environments.

IV. EQUIVALENT CIRCUIT

A simple circuit model explains the observed phenomenon and yields a design law for preventing frequency shift with other loop geometries. The free-space loop can be represented by the network of Fig. 4. Circuit element values can be selected to match the full-wave model impedance data at the operating frequency ω_c as follows. First, the self-resonant frequency ω_0 of the loop in free-space is calculated via the full-wave model. Next, the full-wave model is solved at the operation frequency ω_c . The equivalent circuit resistance R_{ckt} and inductance L_{ckt} are chosen to match the full-wave model resistance R_{loop} and reactance $X_{loop} = \omega_c L_{loop}$ at ω_c using the following approximations:

$$R_{ckt} \sim R_{loop} (1 - \omega_c^2 / \omega_0^2)^2, \quad (1)$$

$$L_{ckt} \sim L_{loop} (1 - \omega_c^2 / \omega_0^2). \quad (2)$$

Finally, the parallel capacitance C_{ckt} is selected according to:

$$C_{ckt} = 1 / (\omega_0^2 L_{ckt}). \quad (3)$$

For the Fig. 1 geometry with $t=7.2$ mm, full-wave simulation indicates the free-space loop resonant frequency is 1.2GHz; with $R_{loop} = 0.122 \Omega$ and $X_{loop} = 90.7 \Omega$ at 433MHz, $R_{ckt} = 0.092 \Omega$ and $L_{ckt} = 29.0$ nH; $C_{ckt} = 0.606$ pF.

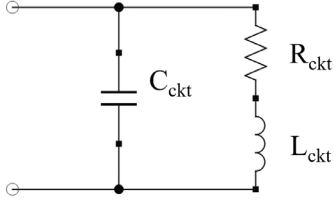


Figure 4. Equivalent circuit of the loop in free-space; no matching circuit is shown.

When the loop is located near a ground plane, the primary perturbation is magnetic flux coupling between the loop and its image in the ground plane, shown in Fig. 5 as a mutual inductance M . The mutual inductance may be calculated from the two-port s-parameters of a mirrored geometry full-wave simulation at a quasi-static frequency (e.g., 10 MHz) as $M = 3.42$ nH. The transformer coupling coefficient $k = M/L_{\text{ckt}} = 0.118$. A “bridging” capacitance represents the parasitic capacitance between the feed node and its ground-plane image, shown in Fig. 5 as C_{br} . Without this circuit element, there is no frequency below self-resonance where the reactances of the free-space and ground-plane equivalent circuits are equal. A simple estimate of C_{br} for the loop of Fig. 1 with $t=7.2$ mm and $z=1.27$ mm is 0.325 pF using the parallel plate capacitor formula.

As shown in Fig. 6(a), a driven circuit simulation is required to calculate the input impedance of the ground plane equivalent circuit because the source image has 180° phase, as dictated by image theory. The antiphase source image causes the equivalent circuit to operate in the “odd” (anti-symmetric) mode only. As illustrated in Fig. 6(b), odd mode operation allows for a greatly simplified ground-plane equivalent circuit that is topologically equivalent to the free-space circuit of Fig. 4, however, the capacitor value is $C_{\text{ckt}} + 2C_{\text{br}}$ and the inductor value is $(1-k)L_{\text{ckt}}$. Using a high Q approximation, we find the reactance of this simplified ground-plane equivalent circuit is equal to that of the free-space equivalent circuit at the operation frequency ω_c when:

$$\omega_c^2 \sim \frac{1}{2} \left(\frac{k}{1-k} \right) \left(\frac{1}{C_{\text{br}} L_{\text{ckt}}} \right). \quad (4)$$

This relation predicts that the equal-reactance frequency decreases as C_{br} is increased (e.g., by increasing t) and as the loop inductance is increased (e.g., by decreasing W) and this is observed in both the full-wave model as well as experimentally.

For 433 MHz, $k = 0.118$, and $L_{\text{ckt}} = 29.0$ nH, (4) indicates C_{br} must be 0.312 pF, in good agreement with the parallel-plate capacitance estimate. Circuit model results are shown in Fig. 7. From (4), we see that only certain combinations of k , C_{br} , and L_{ckt} yield equal reactance at the operating frequency. Thus, for a given loop design, stable tuning occurs only for a particular ground plane separation z . Because C_{br} is influenced by the presence of a dielectric radome (which naturally fixes z when the loop is placed on a ground plane), its effect should be

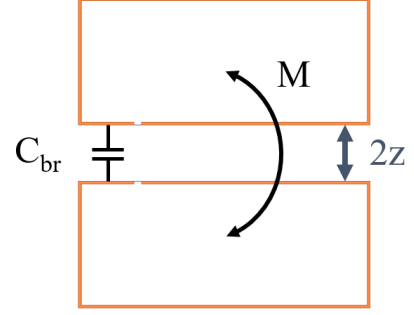


Figure 5. Loop antenna (top) and its ground-plane image (bottom) separated by a distance $2z$. Mutual inductance M between the loops and parasitic capacitance C_{br} between the feeds are indicated.

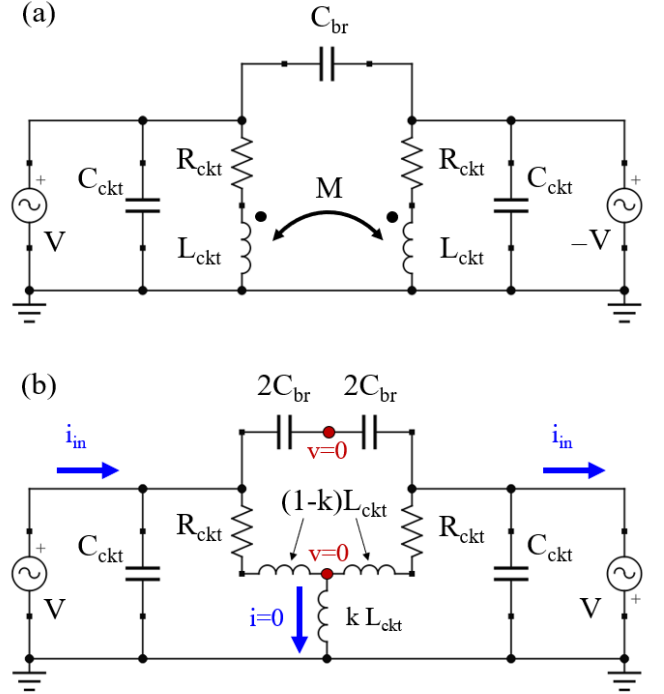


Figure 6. (a) equivalent circuit of the loop near a ground plane, and (b) modified equivalent circuit; image theory dictates an antiphase source image and thus odd (anti-symmetric) mode operation resulting in zero shunt inductor current and zero potential at the nodes indicated. No matching circuit is shown.

accounted for via full-wave simulation. However, the principles of the technique remain unchanged.

V. IMPLEMENTATION AND TESTING

The loop of Fig. 1 with $t=7.2$ mm was fabricated and placed $z=1.27$ mm away from a large conducting ground plane and matched to 50Ω at 433 MHz using RF chip capacitors. The reflection coefficient was measured on a ground plane via a vector network analyzer whose cable was arranged to minimally couple to the antenna loop. A hemispherical Wheeler cap measurement of the matched loop yields 40% radiation efficiency.

Next, a miniature, battery-powered swept-frequency source with constant-available RF power in 50Ω was set inside the

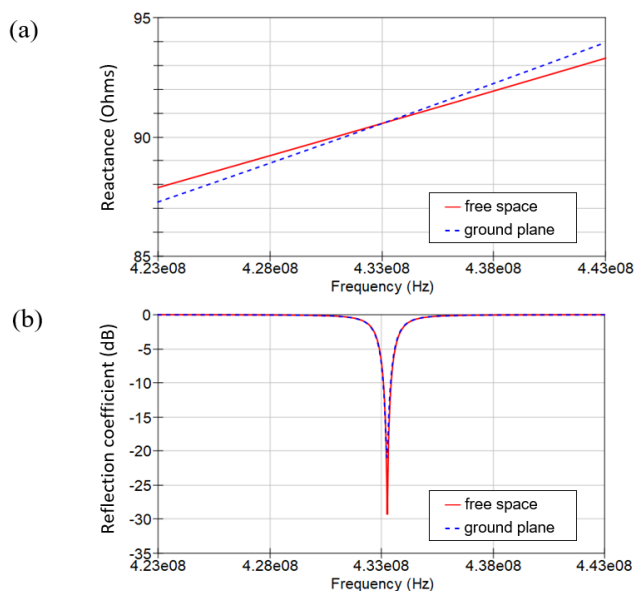


Figure 7. Circuit model results for free-space and $z=1.27$ mm above ground plane, with C_{br} tuned to 0.305 pF. (Top) unmatched loop reactance and (bottom) reflection coefficient with 4.17 pF in series with 148 pF capacitive matching network. The circuit model shows equal-reactance at 433 MHz and resulting zero frequency shift.

loop. The RF signal transmitted by the loop was monitored with a polarization-matched, sub-resonant monopole probe connected to a spectrum analyzer located about 600 mm away from the loop antenna. This was done with the loop in three ground plane configurations: 1) $z=1.27$ mm away from the ground plane, 2) $z=75$ mm away from the ground plane, and 3) with no ground plane; results are presented in Fig. 8. When $z=75$ mm, the loop impedance is close to that in a true free-space environment, however, the radiation pattern remains similar to the $z=1.27$ mm case. Little difference in the received peak amplitude and frequency was observed between configurations 1 and 2. When the ground plane is removed entirely, the radiation pattern changes significantly (now a full toroid covering 4π steradians) and the signal is expected to decrease 3 dB due to this effect. Moreover, the full-wave calculation predicts 1.25 dB decrease in radiation efficiency when moving from $z=1.27$ mm away from ground plane to free space. The measured signal decreased 4.5 dB, with little frequency shift. Thus, we estimate the change in mismatch loss at the feed between free-space and ground plane environments is about 0.25 dB in practice.

VI. CONCLUSION

This paper presents a general design principle for preventing detuning when loop antennas are used both in free space and a fixed distance away from ground planes. The approach balances the inductive and capacitive parasitics introduced by the ground plane such that the resonant frequency remains unchanged. This completely passive technique has none of the cost, size, complexity, RF loss, or DC power consumption drawbacks associated with active antenna tuning approaches. The design

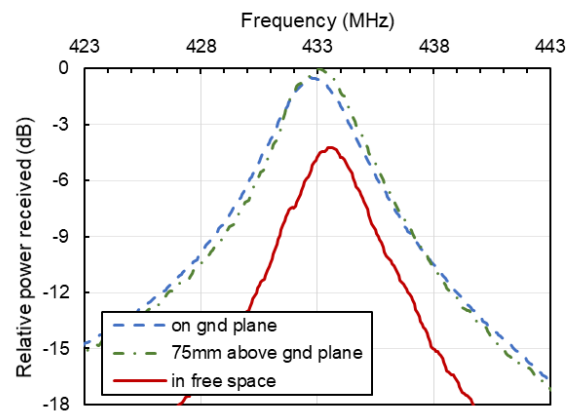


Figure 8. Experimental power received from the transmitting loop antenna with $t=7.2$ mm in three environments demonstrating minimal frequency shift and limited change in peak amplitude. Accounting for expected changes in radiation pattern and radiation efficiency between the ground plane and free-space environments, we estimate the change in mismatch loss to be about 0.25 dB.

may be easily adapted to commercial RFID applications via flexible printed circuit board fabrication and adjustment of the matching network to give a complex conjugate match to passive RFID integrated circuits.

ACKNOWLEDGMENT

The author gratefully acknowledges the contributions of Steve Dunlap, Craig Bennett, Leonard Dixon, Stephanie Otts, Cory Ottesen, Luke Feldner and Dylan Crocker to this work.

REFERENCES

- [1] G. Marrocco, "The art of UHF RFID antenna design: impedance-matching and size-reduction techniques," *IEEE Antennas and Propagation Magazine*, vol. 50, no. 1, pp. 66-79, Feb. 2008.
- [2] T. Björninen, L. Sydänheimo, L. Ukkonen and Y. Rahmat-Samii, "Advances in antenna designs for UHF RFID tags mountable on conductive items," *IEEE Antennas and Propagation Magazine*, vol. 56, no. 1, pp. 79-103, Feb. 2014.
- [3] K. V. S. Rao, S. F. Lam and P. V. Nikitin, "Wideband metal mount UHF RFID tag," *2008 IEEE Antennas and Propagation Society International Symposium*, San Diego, CA, 2008, pp. 1-4.
- [4] K. H. Lee *et al.*, "Design of a UHF RFID metal tag for long reading range using a cavity structure," *2008 Asia-Pacific Microwave Conference*, Macau, 2008, pp. 1-4.
- [5] B. Gao and M. M. F. Yuen, "Passive UHF RFID Packaging With Electromagnetic Band Gap (EBG) Material for Metallic Objects Tracking," *IEEE Transactions on Components, Packaging and Manufacturing Technology*, vol. 1, no. 8, pp. 1140-1146, Aug. 2011.
- [6] B. Yu, S.-J. Kim, B. Jung, F. J. Harackiewicz, and B. Lee. "RFID tag antenna using two-shortened microstrip patches mountable on metallic objects." in *Microwave and Optical Technology Letters* 49, no. 2 (2007): 414-416.
- [7] R. A. Ramirez, E. A. Rojas-Nastrucci and T. M. Weller, "UHF RFID Tags for On-/Off-Metal Applications Fabricated Using Additive Manufacturing," *IEEE Antennas and Wireless Propagation Letters*, vol. 16, pp. 1635-1638, 2017.
- [8] N. A. Mohammed, M. Sivakumar and D. D. Deavours, "An RFID tag capable of free-space and on-metal operation," *2009 IEEE Radio and Wireless Symposium*, San Diego, CA, 2009, pp. 63-66.
- [9] T. Koo, D. Kim, J. Ryu, H. Seo, J. Yook and J. Kim, "Design of a Label-Typed UHF RFID Tag Antenna for Metallic Objects," *IEEE Antennas and Wireless Propagation Letters*, vol. 10, pp. 1010-1014, 2011.
- [10] Patent Pending: U.S. Patent Application Serial No. 16/127,577, filed September 11, 2018.